Journal of Computational Physics 249 (2013) 216–232

Contents lists available at SciVerse ScienceDirect

Journal of Computational Physics

journal homepage: www.elsevier.com/locate/jcp

An adaptive edge finite element method for electromagnetic cloaking simulation ☆

Jichun Li [a,b,*], Yunqing Huang [a], Wei Yang [a]

[a] Hunan Key Laboratory for Computation and Simulation in Science and Engineering, Xiangtan University, China
[b] Department of Mathematical Sciences, University of Nevada, Las Vegas, Las Vegas, NV 89154-4020, USA

ARTICLE INFO

Article history:
Received 16 October 2012
Received in revised form 2 February 2013
Accepted 17 April 2013
Available online 10 May 2013

Keywords:
Maxwell's equations
Invisibility cloak
Finite element method

ABSTRACT

In this paper we develop an adaptive edge finite element method based on a reliable and efficient recovery type a posteriori error estimator for time-harmonic Maxwell equations. The asymptotically exact a posteriori error estimator is based on the superconvergence result proved for the lowest-order edge element on triangular grids, where most pairs of triangles sharing a common edge form approximate parallelograms. The efficiency and robustness of the proposed method is demonstrated by extensive numerical experiments for electromagnetic cloaking problems with highly anisotropic permittivity and permeability.

1. Introduction

In early 2006, Pendry et al. [33] and Leonhardt [24] independently presented the blueprints for making objects invisible to electromagnetic waves by using metamaterials. The basic idea is to use the Maxwell equations' form invariant property to design the permittivty and permeability of the metamaterial. The cloaked region is surrounded by this cloaking metamaterial, and the light will be guided around the cloaked region as if nothing were there. In late 2006, the first practical realization of such a cloak was demonstrated by Schurig et al. [35] over a band of microwave frequencies for a 2-D cloak constructed using artificially structured metamaterials. At present, there is a tremendous interest in the study of invisibility cloaks and their striking applications. We refer readers to (e.g., [8,15,16,29,23,28,30]) for more details about this rapidly growing field and more complete literature.

Numerical simulation plays a very important role in designing the invisibility cloaks and validating theoretical predictions. Due to its flexibility in handling complex geometrical domains and its solid mathematical theory, the finite element method (FEM) is one of the most popular techniques in solving electromagnetic wave propagation problems. To date, the FEM cloaking simulation seems to be dominated by the commercial package COMSOL. To our best knowledge, not much research has been devoted to developing more efficient and robust FEMs for cloaking simulation. In 2011, Zhai et al. [40] developed an efficient finite element method for solving 3D axisymmetrical invisibility cloaks and concentrators. Recently, Demkowicz and Li [12] extended the Discontinuous Petrov–Galerkin (DPG) method to show the effectiveness of the DPG method in cloak simulations. Some simple *h*-adaptivity has been introduced for our DPG method, however theoretical justification of the effectiveness of *h*-adaptive was not investigated there.

☆ Work supported by NSFC project 11271310, NSFC Key Project 11031006, IRT1179 of PCSIRT and MOST 2010DFR00700, National Science Foundation Grant DMS-0810896, and Hunan Provincial Innovation Foundation for Postgraduate (CX201243).

* Corresponding author at: Department of Mathematical Sciences, University of Nevada, Las Vegas, Las Vegas, NV 89154-4020, USA.
E-mail addresses: jichun@unlv.nevada.edu (J. Li), huangyq@xtu.edu.cn (Y. Huang), yangweixtu@126.com (W. Yang).

0021-9991/$ - see front matter © 2013 Elsevier Inc. All rights reserved.
http://dx.doi.org/10.1016/j.jcp.2013.04.026

In this paper, a reliable and efficient recovery type a posteriori error estimator is developed for time-harmonic Maxwell's equations. Our estimator is the so-called recovery type, which was originally introduced by Zienkiewicz and Zhu [42] and has been extensively developed and analyzed by various authors [38,39] for many partial differential equations except Maxwell's equations. More specifically, our error estimator is based on the superconvergence result obtained for time-harmonic Maxwell's equations solved by the lowest order triangular edge element. Comparing to those existing superconvergence results for Maxwell's equations (e.g., [17,34], [32, p. 201], and [[27, Ch. 5]), our superconvergence result is original. We then use this a posteriori error estimator in our adaptive edge element method and the effectiveness is demonstrated by several cloaking simulations. We like to remark that there are some excellent works on a posteriori error estimators [4,7,9,10,41] and adaptive FEM [1,11,21,36] for Maxwell's equations, but they are mainly the residual types for a simple medium such as vacuum and have not used for such complicated problems as our cloaking simulations.

The rest of the paper is organized as follows. In Section 2, we provide the superconvergence analysis for time-harmonic Maxwell's equations solved by the lowest order triangular edge element. Then in Section 3, we apply the superconvergence result to derive the recovery type a posteriori error estimator, and use the error estimator to develop an adaptive finite element method for electromagnetic cloaking simulations. Extensive numerical experiments are presented in Section 4 to justify our theoretical analysis and demonstrate the effectiveness of our adaptive method. We conclude the paper in Section 5.

2. Superconvergence analysis for time-harmonic Maxwell's equations

First let us introduce some common notations. We assume that Ω is a bounded and simply connected Lipschitz polyhedron of R^d ($d = 2$ or 3) with connected boundary $\partial\Omega$ and unit outward normal $\boldsymbol{n}$. For $m, p \geqslant 1$, we denote the standard Sobolev space by $W^{m,p}(\Omega)$. When $p = 2$, we usually write $H^m(\Omega) = W^{m,2}(\Omega)$. Furthermore, we need some other Sobolev spaces:

$$H_0(curl;\Omega) = \{\boldsymbol{v} \in (L^2(\Omega))^d; \quad \nabla \times \boldsymbol{v} \in (L^2(\Omega))^d, \ \boldsymbol{n} \times \boldsymbol{v} = \boldsymbol{0} \text{ on } \partial\Omega\},$$
$$H^s(curl;\Omega) = \{\boldsymbol{v} \in (H^s(\Omega))^d; \quad \nabla \times \boldsymbol{v} \in (H^s(\Omega))^d\}, \ \forall s > 0.$$

The above spaces are equipped with norms

$$||\boldsymbol{v}||_{H(curl;\Omega)} = (||\boldsymbol{v}||_0^2 + ||\nabla \times \boldsymbol{v}||_0^2)^{1/2} \quad \forall \boldsymbol{v} \in H_0(curl;\Omega),$$
$$||\boldsymbol{v}||_{H^s(curl;\Omega)} = (||\boldsymbol{v}||_{H^s(\Omega)}^2 + ||\nabla \times \boldsymbol{v}||_{H^s(\Omega)}^2)^{1/2} \quad \forall \boldsymbol{v} \in H^s(curl;\Omega),$$

where $||\cdot||_{0,\Omega}$ (or simply $||\cdot||_0$) denotes the $(L^2(\Omega))^d$ norm.

2.1. The modeling equations and some preliminaries

Modeling of electromagnetic phenomena at a fixed frequency ω is governed by the full Maxwell's equations:

$$\nabla \times \boldsymbol{E} + i\omega\mu\boldsymbol{H} = \boldsymbol{0}, \quad \text{in } \Omega, \tag{2.1}$$
$$\nabla \times \boldsymbol{H} - i\omega\varepsilon\boldsymbol{E} = \boldsymbol{J}, \quad \text{in } \Omega, \tag{2.2}$$

where $i = \sqrt{-1}$, $\boldsymbol{E}(\boldsymbol{x})$ and $\boldsymbol{H}(\boldsymbol{x})$ are the electric and magnetic fields, ε and μ are the permittivity and permeability of the material, and $\boldsymbol{J}$ is the applied current density.

Eliminating $\boldsymbol{H}$ from (2.1) and (2.2), we obtain

$$\nabla \times (\mu^{-1}\nabla \times \boldsymbol{E}) - \omega^2\varepsilon\boldsymbol{E} = -i\omega\boldsymbol{J} \quad \text{in } \Omega. \tag{2.3}$$

Let us denote the wavenumber $k = \omega\sqrt{\varepsilon\mu}$. To avoid the technicality and simplify the presentation, we assume that ϵ and μ are constants, in which case we can simplify the problem (2.3) to:

$$\nabla \times (\nabla \times \boldsymbol{E}) - k^2\boldsymbol{E} = \boldsymbol{F} \equiv -i\omega\mu\boldsymbol{J} \quad \text{in } \Omega. \tag{2.4}$$

Moreover, we assume that the problem (2.4) is subject to the perfectly conducting (PEC) boundary condition

$$\boldsymbol{n} \times \boldsymbol{E} = \boldsymbol{0} \quad \text{on } \partial\Omega. \tag{2.5}$$

The variational formulation of the problem (2.4) and (2.5) is to find $\boldsymbol{E} \in H_0(curl;\Omega)$ such that

$$a(\boldsymbol{E},\boldsymbol{\phi}) = (\boldsymbol{F},\boldsymbol{\phi}) \quad \forall \boldsymbol{\phi} \in H_0(curl;\Omega), \tag{2.6}$$

where

$$a(\boldsymbol{E},\boldsymbol{\phi}) = (\nabla \times \boldsymbol{E}, \nabla \times \boldsymbol{\phi}) - k^2(\boldsymbol{E},\boldsymbol{\phi}). \tag{2.7}$$

Here and below $(\cdot,\cdot)$ denotes the inner product in $(L^2(\Omega))^d$.

To design a finite element method, we assume that Ω is partitioned by a regular mesh T_h of tetrahedra in R^3 (or triangles in R^2), where h is the mesh size. Due to the low regularity of the solution for Maxwell's equations, we just consider the lowest-order Nédélec curl conforming element (often called edge element) space:

$$\boldsymbol{V}_h = \{\boldsymbol{\phi}_h \in H_0(curl;\Omega): \quad \boldsymbol{\phi}_h|_K = \text{span}\{\lambda_i\nabla\lambda_j - \lambda_j\nabla\lambda_i\}, \ \forall K \in T_h\}, \tag{2.8}$$

where λ_i denotes the barycentric coordinate at the ith vertex of the tetrahedron or triangle K.

Now we can define the standard finite element method for solving the problem (2.4) and (2.5): Find $\boldsymbol{E}_h \in \boldsymbol{V}_h$ such that

$$a(\boldsymbol{E}_h, \boldsymbol{\phi}_h) = (\boldsymbol{F}, \boldsymbol{\phi}_h) \quad \forall \boldsymbol{\phi}_h \in \boldsymbol{V}_h. \tag{2.9}$$

Denote the solution error $\boldsymbol{e}_h = \boldsymbol{E} - \boldsymbol{E}_h$. The following lemmas present the well-posedness of the problem (2.6) and some fundamental error estimates.

Theorem 2.1 [32]. *Assume that Ω is a bounded and simply connected Lispschitz polyhedron with connected boundary, and $\boldsymbol{E}$ and $\boldsymbol{E}_h$ satisfy (2.6) and (2.9), respectively. If k is not an interior Maxwell eigenvalue, then the variational problem (2.6) has a unique solution $\boldsymbol{E} \in H_0(curl;\Omega)$ such that*

$$||\boldsymbol{E}||_{H(curl;\Omega)} \leqslant C||\boldsymbol{F}||_0,$$

where the constant $C > 0$ is independent of $\boldsymbol{E}$ and $\boldsymbol{F}$ but dependent on k. Moreover, if $\boldsymbol{E} \in H^1(curl;\Omega)$, then there exists a constant $C > 0$ independent of h such that

$$||\boldsymbol{E} - \boldsymbol{E}_h||_{H(curl;\Omega)} \leqslant Ch||\boldsymbol{E}||_{H^1(curl;\Omega)}.$$

Lemma 2.1 [32, Lemma 7.7]. *For sufficiently small h, there exist constants $C > 0$ and $\delta \in (0, \frac{1}{2}]$ such that*

$$\sup_{\boldsymbol{v}_h \in \boldsymbol{V}_h} \frac{|(\boldsymbol{e}_h, \boldsymbol{v}_h)|}{||\boldsymbol{v}_h||_{H(curl;\Omega)}} \leqslant Ch^{\delta+1/2}||\boldsymbol{e}_h||_{H(curl;\Omega)}.$$

2.2. Superclose analysis for the lowest-order triangular edge element

Let us denote $\boldsymbol{u}_I \in \boldsymbol{V}_h$ for the standard Nédélec interpolation operator of $\boldsymbol{u}$. For the lowest-order triangular edge element, we can write

$$\boldsymbol{u}_I|_K(x,y) = \sum_{j=1}^{3}\left(\int_{l_j} \boldsymbol{u}\cdot\boldsymbol{\tau}_j dl\right)\boldsymbol{N}_j(x,y) \quad \forall K \in T_h, \tag{2.10}$$

where $\boldsymbol{\tau}_j$ is the unit tangent vector on edge l_j, and $\boldsymbol{N}_j$ is the corresponding basis function.

Using the Stoke's formula and the definition of $\boldsymbol{u}_I$, we have.

Lemma 2.2. *For any function $\boldsymbol{u} \in H(curl;\Omega)$, we have*

$$\int_K \nabla \times (\boldsymbol{u} - \boldsymbol{u}_I)dxdy = 0 \quad \forall K \in T_h.$$

For a triangular mesh formed by parallelograms, we have the following elementwise superclose identity.

Lemma 2.3 [18, Theorem 3.3]. *Assume that the domain Ω is covered by a triangular mesh formed by parallelograms. On any parallelogram $\Diamond$, for any function $\boldsymbol{u} \in (H^3(\Diamond))^2$ and $\boldsymbol{\phi}_h \in V_h$, then we have*

$$\int_\Diamond (\boldsymbol{u} - \boldsymbol{u}_I)\boldsymbol{\phi}_h dxdy \leqslant Ch^2||\boldsymbol{u}||_{(H^3(\Diamond))^2}||\boldsymbol{\phi}_h||_{0,\Diamond}.$$

Lemma 2.4. *Assume that the domain Ω is covered by a triangular mesh formed by parallelograms, and $\boldsymbol{E}$ and $\boldsymbol{E}_h$ satisfy (2.6) and (2.9), respectively. If h is sufficiently small, then there exist constants $C > 0$ and $\delta \in (0, 1/2]$ such that*

$$||\boldsymbol{E}_I - \boldsymbol{E}_h||_{H(curl;\Omega)} \leqslant C\left(h^2||\boldsymbol{E}||_{(H^3(\Omega))^2} + h^{\delta+1/2}||e_h||_{H(curl;\Omega)}\right). \tag{2.11}$$

Proof. Let $\boldsymbol{\phi}_h = \boldsymbol{E}_I - \boldsymbol{E}_h$. From (2.7), we have

$$\begin{aligned}
||\boldsymbol{\phi}_h||^2_{H(curl;\Omega)} &= a(\boldsymbol{\phi}_h, \boldsymbol{\phi}_h) + (1+k^2)(\boldsymbol{\phi}_h, \boldsymbol{\phi}_h) \\
&= a(\boldsymbol{E}_I - \boldsymbol{E}, \boldsymbol{\phi}_h) + a(\boldsymbol{E} - \boldsymbol{E}_h, \boldsymbol{\phi}_h) + (1+k^2)(\boldsymbol{\phi}_h, \boldsymbol{\phi}_h) \\
&= a(\boldsymbol{E}_I - \boldsymbol{E}, \boldsymbol{\phi}_h) + (1+k^2)(\boldsymbol{\phi}_h, \boldsymbol{\phi}_h) \\
&= (\nabla \times (\boldsymbol{E}_I - \boldsymbol{E}), \nabla \times \boldsymbol{\phi}_h) + (\boldsymbol{E}_I - \boldsymbol{E}, \boldsymbol{\phi}_h) + (1+k^2)(\boldsymbol{E} - \boldsymbol{E}_h, \boldsymbol{\phi}_h) \\
&= \sum_{i=1}^{3} Err_i.
\end{aligned} \tag{2.12}$$

Note that $\nabla \times \boldsymbol{\phi}_h$ is a constant on each element, using Lemma 2.2 we easily have

$$Err_1 = (\nabla \times (\boldsymbol{E}_I - \boldsymbol{E}), \nabla \times \boldsymbol{\phi}_h) = 0. \tag{2.13}$$

Using Lemma 2.3, we immediately have

$$Err_2 = (\boldsymbol{E}_I - \boldsymbol{E}, \boldsymbol{\phi}_h) \leqslant Ch^2 ||\boldsymbol{E}||_{(H^3(\Omega))^2} ||\boldsymbol{\phi}_h||_{0,\Omega}. \tag{2.14}$$

Finally, using Lemma 2.1, we have

$$\begin{aligned} Err_3 &= (1+k^2)(\boldsymbol{E} - \boldsymbol{E}_h, \boldsymbol{\phi}_h) \\ &\leqslant C \sup_{v_h \in V_h} \frac{|(e_h, v_h)|}{||v_h||_{H(curl;\Omega)}} ||E_I - E_h||_{H(curl,\Omega)} \\ &\leqslant Ch^{\delta+1/2} ||e_h||_{H(curl;\Omega)} ||E_I - E_h||_{H(curl,\Omega)}. \end{aligned} \tag{2.15}$$

The proof is completed by substituting (2.13)–(2.15) into (2.12). □

Note that the estimate (2.11) is a superclose result between the interpolation $\boldsymbol{E}_I$ and the finite element solution $\boldsymbol{E}_h$, since by Theorem 2.1 we only have $||\boldsymbol{E} - \boldsymbol{E}_h||_{H(curl;\Omega)} \leqslant Ch$, which is one order less than $||\boldsymbol{E}_I - \boldsymbol{E}_h||_{H(curl;\Omega)}$.

Let us introduce the discrete l_2 norm $|\boldsymbol{u}|_{l_2,\Omega} = \left(\frac{1}{N_e} \sum_{K \in T_h} \sum_{\boldsymbol{x}_e \in K} |\boldsymbol{u}(\boldsymbol{x}_e)|^2\right)^{1/2}$, where $\boldsymbol{x}_e$ is the midpoint of the interior edge e and N_e is the total number of interior edges. Moreover, let the averaging operator $R(\boldsymbol{u}(\boldsymbol{x}_e)) = (\boldsymbol{u}(\boldsymbol{x}_e)|_{K_1} + \boldsymbol{u}(\boldsymbol{x}_e)|_{K_2})/2$, where K_1 and K_2 are the two triangles sharing the middle edge point $\boldsymbol{x}_e$.

Extending Lemma 2.4, we can have the following superclose result.

Lemma 2.5. *Under the same assumption as Lemma 2.4, for sufficiently small h, there exist constants $C > 0$ and $\delta \in (0, 1/2]$ such that*

(i) $|R(\boldsymbol{E}_I - \boldsymbol{E}_h)|_{l_2,\Omega} \leqslant C\left(h^2 ||\boldsymbol{E}||_{(H^3(\Omega))^2} + h^{\delta+1/2} ||e_h||_{H(curl;\Omega)}\right)$,
(ii) $|R(\nabla \times (\boldsymbol{E}_I - \boldsymbol{E}_h))|_{l_2,\Omega} \leqslant C\left(h^2 ||\boldsymbol{E}||_{(H^3(\Omega))^2} + h^{\delta+1/2} ||e_h||_{H(curl;\Omega)}\right)$.

Proof. Let $\boldsymbol{\phi}_h = \boldsymbol{E}_I - \boldsymbol{E}_h$, and $S_\tau = O(\frac{|\Omega|}{N})$ be the area of the element τ, where N denotes the total number of the elements in the mesh T_h.

Using the quadrature identity (cf. [25, p.194]):

$$\int_\tau \psi(x,y)dxdy = \frac{S_\tau}{3} \sum_{i=1}^{3} \psi(\boldsymbol{x}_{e_i}) \quad \forall \psi \in P_2(\tau)$$

and the fact that $\boldsymbol{\phi}_h$ is linear on each element τ, we have

$$\sum_{\tau \in T_h} \sum_{\boldsymbol{x}_e \in \tau} R^2(\boldsymbol{\phi}_h(\boldsymbol{x}_e)) \cdot S_\tau/3 \leqslant \sum_{\tau} \sum_{i=1}^{3} \phi_h^2(\boldsymbol{x}_e) \cdot S_\tau/3 = \int_\Omega \phi_h^2 dxdy,$$

which along with the fact $\frac{N_e}{N} = O(1)$ yields

$$\sum_{\tau \in T_h} \sum_{\boldsymbol{x}_e \in \tau} \frac{R^2(\boldsymbol{\phi}_h(\boldsymbol{x}_e))}{N_e} = \sum_{\tau \in T_h} \sum_{\boldsymbol{x}_e \in \tau} R^2(\boldsymbol{\phi}_h(\boldsymbol{x}_e)) \cdot \frac{S_\tau}{3} \cdot O\left(\frac{3N}{|\Omega| N_e}\right) \leqslant C \int_\Omega \phi_h^2 dxdy.$$

Finally, using Lemma 2.4, we easily obtain

$$|R(\boldsymbol{E}_I - \boldsymbol{E}_h)|_{l_2,\Omega} = \left(\sum_{\tau \in T_h} \sum_{\boldsymbol{x}_e \in \tau} \frac{R^2(\boldsymbol{\phi}_h(\boldsymbol{x}_e))}{N_e}\right)^{1/2} \leqslant C||\boldsymbol{\phi}_h||_{0,\Omega} \leqslant C\left(h^2 ||\boldsymbol{E}||_{(H^3(\Omega))^2} + h^{\delta+1/2} ||e_h||_{H(curl;\Omega)}\right),$$

which completes the proof of (i). Applying the same technique to $\boldsymbol{\phi}_h = \nabla \times (\boldsymbol{E}_I - \boldsymbol{E}_h)$, we can prove (ii). □

2.3. Superconvergence analysis for the lowest-order triangular edge element

In this section, we will use the superclose results obtained in last section to prove some superconvergence results for the time-harmonic Maxwell's equations solved by the lowest-order triangular edge element.

First, we present a result on line integrals.

Lemma 2.6. *Consider a parallelogram formed by vertices A–D, where $\boldsymbol{x}_e = (x_c, y_c)$ is the midpoint of AC, $\alpha = \angle BAC$, and $2l_1$ and $2l_3$ denote the lengths of AB and AC, respectively (see Fig. 2.1). Furthermore, let $\boldsymbol{\tau}_{ij}$ denote the unit tangent vector along edge ij, where $i,j = A,B,C,D$. Then for any function $\boldsymbol{u} = (u_1,u_2)^T \in (W^{3,\infty}(\Omega))^2$, we have*

$$(i)\quad \int_{AC} \boldsymbol{u}\cdot\boldsymbol{\tau}_{AC}ds = 2l_3\cos\alpha u_1(\boldsymbol{x}_e) + \frac{(l_3\cos\alpha)^3}{3}\partial_{xx}u_1(\boldsymbol{x}_e) + \frac{2l_3^3\sin\alpha\cos^2\alpha}{3}\partial_{xy}u_1(\boldsymbol{x}_e) + \frac{l_3^3\sin^2\alpha\cos\alpha}{3}\partial_{yy}u_1(\boldsymbol{x}_e) + 2l_3 \times \sin\alpha u_2(\boldsymbol{x}_e) + \frac{l_3^3\sin\alpha\cos^2\alpha}{3}\partial_{xx}u_2(\boldsymbol{x}_e) + \frac{2l_3^3\sin^2\alpha\cos\alpha}{3}\partial_{xy}u_2(\boldsymbol{x}_e) + \frac{l_3^3\sin^3\alpha}{3}\partial_{yy}u_2(\boldsymbol{x}_e) + O(h^4),$$

$$(ii)\quad \int_{CD} \boldsymbol{u}\cdot\boldsymbol{\tau}_{CD}ds = -2l_1u_1(\boldsymbol{x}_e) + 2(l_1^2 - l_1l_3\cos\alpha)\partial_x u_1(\boldsymbol{x}_e) - 2l_1l_3\sin\alpha\partial_y u_1(\boldsymbol{x}_e) + (2l_1^2l_3\cos\alpha - \frac{4l_3^3}{3} - l_1l_3^2 \times \cos^2\alpha)\partial_{xx}u_1(\boldsymbol{x}_e) + 2(l_1^2l_3\sin\alpha - l_1l_3^2\cos\alpha\sin\alpha)\partial_{xy}u_1(\boldsymbol{x}_e) - l_1l_3^2\sin^2\alpha\partial_{yy}u_1(\boldsymbol{x}_e) + O(h^4),$$

$$(iii)\quad \int_{DA} \boldsymbol{u}\cdot\boldsymbol{\tau}_{DA}ds = 2(l_1 - l_3\cos\alpha)u_1(\boldsymbol{x}_e) + 2(l_1l_3\cos\alpha - l_1^2)\partial_x u_1(\boldsymbol{x}_e) + \frac{l_1 - l_3\cos\alpha}{3}(4l_1^2 - 2l_1l_3\cos\alpha + l_3^2 \times \cos^2\alpha)\partial_{xx}u_1(\boldsymbol{x}_e) + \frac{l_1 - l_3\cos\alpha}{3}(2l_3^2\cos\alpha\sin\alpha - 2l_1l_3\sin\alpha)\partial_{xy}u_1(\boldsymbol{x}_e) + \frac{l_1 - l_3\cos\alpha}{3}(l_3^2 \times \sin^2\alpha)\partial_{yy}u_1(\boldsymbol{x}_e) - 2l_3\sin\alpha u_2(\boldsymbol{x}_e) + 2l_1l_3\sin\alpha\partial_x u_2(\boldsymbol{x}_e) - \frac{l_3\sin\alpha}{3}(4l_1^2 - 2l_1l_3\cos\alpha + l_3^2 \times \cos^2\alpha)\partial_{xx}u_2(\boldsymbol{x}_e) - \frac{l_3\sin\alpha}{3}(2l_3^2\cos\alpha\sin\alpha - 2l_1l_3\sin\alpha)\partial_{xy}u_2(\boldsymbol{x}_e) - \frac{l_3\sin\alpha}{3}(l_3^2\sin^2\alpha)\partial_{yy}u_2(\boldsymbol{x}_e) + O(h^4),$$

$$(iv)\quad \int_{AB} \boldsymbol{u}\cdot\boldsymbol{\tau}_{AB}ds = 2l_1u_1(\boldsymbol{x}_e) + 2(l_1^2 - l_1l_3\cos\alpha)\partial_x u_1(\boldsymbol{x}_e) - 2l_1l_3\sin\alpha\partial_y u_1(\boldsymbol{x}_e) + \left(\frac{4l_3^3}{3} - 2l_1^2l_3\cos\alpha + l_1l_3^2\cos^2\alpha\right)\partial_{xx}u_1(\boldsymbol{x}_e) - 2(l_1^2l_3\sin\alpha - l_1l_3^2\cos\alpha\sin\alpha)\partial_{xy}u_1(\boldsymbol{x}_e) + l_1l_3^2 \times \sin^2\alpha\partial_{yy}u_1(\boldsymbol{x}_e) + O(h^4),$$

$$(v)\quad \int_{BC} \boldsymbol{u}\cdot\boldsymbol{\tau}_{BC}ds = 2(l_3\cos\alpha - l_1)u_1(\boldsymbol{x}_e) + 2(l_1l_3\cos\alpha - l_1^2)\partial_x u_1(\boldsymbol{x}_e) + \frac{l_3\cos\alpha - l_1}{3}(4l_1^2 - 2l_1l_3\cos\alpha + l_3^2 \times \cos^2\alpha)\partial_{xx}u_1(\boldsymbol{x}_e) + \frac{l_3\cos\alpha - l_1}{3}(2l_3^2\cos\alpha\sin\alpha - 2l_1l_3\sin\alpha)\partial_{xy}u_1(\boldsymbol{x}_e) + \frac{l_3\cos\alpha - l_1}{3}(l_3^2 \times \sin^2\alpha)\partial_{yy}u_1(\boldsymbol{x}_e) + 2l_3\sin\alpha u_2(\boldsymbol{x}_e) + 2l_1l_3\sin\alpha\partial_x u_2(\boldsymbol{x}_e) + \frac{l_3\sin\alpha}{3}(4l_1^2 - 2l_1l_3\cos\alpha + l_3^2 \times \cos^2\alpha)\partial_{xx}u_2(\boldsymbol{x}_e) + \frac{l_3\sin\alpha}{3}(2l_3^2\cos\alpha\sin\alpha - 2l_1l_3\sin\alpha)\partial_{xy}u_2(\boldsymbol{x}_e) + \frac{l_3\sin\alpha}{3}(l_3^2\sin^2\alpha)\partial_{yy}u_2(\boldsymbol{x}_e) + O(h^4).$$

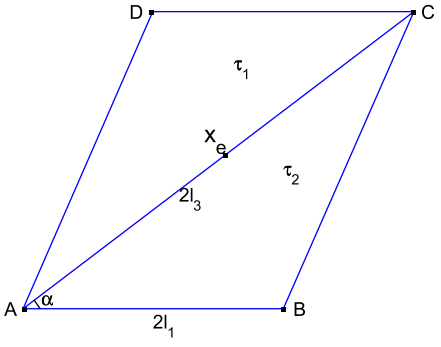

Fig. 2.1. The exemplary parallelogram.

Proof.

(i) Using $\boldsymbol{\tau}_{AC} = (\cos\alpha, \sin\alpha)$, we have

$$\int_{AC} \boldsymbol{u}\cdot\boldsymbol{\tau}_{AC} ds = \int_{x_A}^{x_C} (u_1 dx + u_2 dy) = \int_{x_A}^{x_C} (u_1 + u_2\tan\alpha) dx. \tag{2.16}$$

Using the Taylor expansions of u_i $(i = 1, 2)$:

$$\begin{aligned} u_i = {} & u_i(\boldsymbol{x}_e) + (x - x_c)\partial_x u_i(\boldsymbol{x}_e) + (y - y_c)\partial_y u_i(\boldsymbol{x}_e) \\ & + \frac{1}{2}\left[(x - x_c)^2\partial_{xx} u_i(\boldsymbol{x}_e) + 2(x - x_c)(y - y_c)\partial_{xy} u_i(\boldsymbol{x}_e) + (y - y_c)^2\partial_{yy} u_i(\boldsymbol{x}_e)\right] + O(h^3) \end{aligned} \tag{2.17}$$

and the equation of line AC: $y = (\tan\alpha)(x - x_c) + y_c$, we have

$$\begin{aligned} \int_{x_A}^{x_C} u_i dx = \int_{x_A}^{x_C} & [u_i(\boldsymbol{x}_e) + (x - x_c)\partial_x u_i(\boldsymbol{x}_e) + \tan\alpha(x - x_c)\partial_y u_i(\boldsymbol{x}_e) + \frac{1}{2}((x - x_c)^2\partial_{xx} u_i(\boldsymbol{x}_e) + 2\tan\alpha(x \\ & - x_c)^2\partial_{xy} u_i(\boldsymbol{x}_e) + \tan^2\alpha(x - x_c)^2\partial_{yy} u_i(\boldsymbol{x}_e)) + O(h^3)] dx. \end{aligned} \tag{2.18}$$

Using the identities

$$\int_{x_A}^{x_C} (x - x_c) dx = \int_{x_c - l_3\cos\alpha}^{x_c + l_3\cos\alpha} (x - x_c) dx = 0,$$

$$\int_{x_A}^{x_C} (x - x_c)^2 dx = \frac{1}{3}(x - x_c)^3 \Big|_{x_c - l_3\cos\alpha}^{x_c + l_3\cos\alpha} = \frac{2l_3^3\cos^3\alpha}{3}$$

and Eqs. (2.16)–(2.18), we finish the proof of (i).

(ii) From $\boldsymbol{\tau}_{CD} = (-1, 0)$, we have

$$\int_{CD} \boldsymbol{u}\cdot\boldsymbol{\tau}_{CD} ds = -\int_{x_D}^{x_C} u_1 dx, \tag{2.19}$$

which, along with (2.17), the equation of line CD: $y = y_c + l_3\sin\alpha$, and the facts

$$\int_{x_D}^{x_C} (x - x_c) dx = \int_{x_c + l_3\cos\alpha - 2l_1}^{x_c + l_3\cos\alpha} (x - x_c) dx = 2l_1 l_3\cos\alpha - 2l_1^2,$$

$$\int_{x_D}^{x_C} (y - y_c) dx = \int_{x_c + l_3\cos\alpha - 2l_1}^{x_c + l_3\cos\alpha} (y_c + l_3\sin\alpha - y_c) dx = 2l_1 l_3\sin\alpha,$$

$$\int_{x_D}^{x_C} (y - y_c)^2 dx = 2l_1(l_3\sin\alpha)^2,$$

$$\int_{x_D}^{x_C} (x - x_c)^2 dx = \int_{x_c + l_3\cos\alpha - 2l_1}^{x_c + l_3\cos\alpha} (x - x_c)^2 dx = 2l_1 l_3^2\cos^2\alpha - 4l_1^2 l_3\cos\alpha + \frac{8}{3}l_1^3,$$

we complete the proof of (ii).

(iii) The proof is completed by using the equation of line DA:

$$x = x_c + l_3\cos\alpha - 2l_1 + (2l_1 - 2l_3\cos\alpha)t,$$
$$y = y_c + l_3\sin\alpha - (2l_3\sin\alpha)t,$$

the Taylor expansion of $u_i (i = 1, 2)$:

$$\begin{aligned} u_i(x, y) = {} & u_i(\boldsymbol{x}_e) + (l_3\cos\alpha - 2l_1 + (2l_1 - 2l_3\cos\alpha)t)\partial_x u_i(\boldsymbol{x}_e) + (l_3\sin\alpha - (2l_3\sin\alpha)t)\partial_y u_i(\boldsymbol{x}_e) + \frac{1}{2}((l_3\cos\alpha - 2l_1 \\ & + (2l_1 - 2l_3\cos\alpha)t)^2\partial_{xx} u_i(\boldsymbol{x}_e) + 2(x - x_c)(l_3\sin\alpha - (2l_3\sin\alpha)t)\partial_{xy} u_i(\boldsymbol{x}_e) + (l_3\sin\alpha - (2l_3 \\ & \times \sin\alpha)t)^2\partial_{yy} u_i(\boldsymbol{x}_e)) + O(h^3) \end{aligned} \tag{2.20}$$

and the identities:

$$\int_0^1 [l_3\cos\alpha - 2l_1 + (2l_1 - 2l_3\cos\alpha)t] dt = -l_1, \quad \int_0^1 [l_3\sin\alpha - (2l_3\sin\alpha)t] dt = 0,$$

$$\int_0^1 [l_3\cos\alpha - 2l_1 + (2l_1 - 2l_3\cos\alpha)t]^2 dt = \frac{4}{3}l_1^2 - \frac{2}{3}l_1 l_3\cos\alpha + \frac{1}{3}l_3^2\cos^2\alpha,$$

$$\int_0^1 [l_3\cos\alpha - 2l_1 + (2l_1 - 2l_3\cos\alpha)t][l_3\sin\alpha - (2l_3\sin\alpha)t]dt = \frac{1}{3}l_3^2\cos\alpha\sin\alpha - \frac{1}{3}l_1l_3\sin\alpha,$$

$$\int_0^1 [l_3\sin\alpha - (2l_3\sin\alpha)t]^2 dt = \frac{1}{3}l_3^2\sin^2\alpha,$$

in the integral

$$\int_{DA} \boldsymbol{u}\cdot\boldsymbol{\tau}_{DA}ds = \int_0^1 [2(l_1 - l_3\cos\alpha)u_1 - 2l_3\sin\alpha u_2]dt.$$

(iv) $\int_{AB}\boldsymbol{u}\cdot\boldsymbol{\tau}_{AB}ds$ can be obtained by a similar argument to (ii).
(v) $\int_{BC}\boldsymbol{u}\cdot\boldsymbol{\tau}_{BC}ds$ can be proved by a similar argument to (iii). □

Using Lemma 2.6, we can prove the following pointwise superconvergence result between the curl of one function and its Nédélec interpolation.

Lemma 2.7. *Under the same assumption as Lemma 2.6, for any function* $\boldsymbol{u} = (u_1, u_2)^T \in (W^{3,\infty}(\Omega))^2$ *and any parallelogram center* $\boldsymbol{x}_e$*, we have*

$$|\nabla\times\boldsymbol{u}(\boldsymbol{x}_e) - R(\nabla\times\boldsymbol{u}_I(\boldsymbol{x}_e))| \leqslant Ch^2.$$

Proof. For the lowest-order triangular edge element basis function $\boldsymbol{\phi}_{ij}$, where $i,j = A,B,C,D$, we have (cf. [18, Lemma 2.1]):

$$(\nabla\times\boldsymbol{\phi}_{AC})(\boldsymbol{x}_e) = (\nabla\times\boldsymbol{\phi}_{CD})(\boldsymbol{x}_e) = (\nabla\times\boldsymbol{\phi}_{DA})(\boldsymbol{x}_e) = 1/S_{\tau_1}, \tag{2.21}$$

By the Nédélec interpolation definition (2.10), and (2.21), we have

$$(\nabla\times\boldsymbol{u}_I)|_{\tau_1}(\boldsymbol{x}_e) = \left[\int_{AC}\boldsymbol{u}\cdot\boldsymbol{\tau}_{AC}ds + \int_{CD}\boldsymbol{u}\cdot\boldsymbol{\tau}_{CD}ds + \int_{DA}\boldsymbol{u}\cdot\boldsymbol{\tau}_{DA}ds\right]\Big/S_{\tau_1}. \tag{2.22}$$

By the same argument, we have

$$(\nabla\times\boldsymbol{u}_I)|_{\tau_2}(\boldsymbol{x}_e) = \left[\int_{AB}\boldsymbol{u}\cdot\boldsymbol{\tau}_{AB}ds + \int_{BC}\boldsymbol{u}\cdot\boldsymbol{\tau}_{BC}ds + \int_{CA}\boldsymbol{u}\cdot\boldsymbol{\tau}_{CA}ds\right]\Big/S_{\tau_2}. \tag{2.23}$$

Taking the average of (2.22) and (2.23), and using the fact $S_{\tau_1} = S_{\tau_2} = 2l_1l_3\sin\alpha$, we obtain

$$R(\nabla\times\boldsymbol{u}_I)(\boldsymbol{x}_e) = \left[\int_{AB}\boldsymbol{u}\cdot\boldsymbol{\tau}_{AB}ds + \int_{BC}\boldsymbol{u}\cdot\boldsymbol{\tau}_{BC}ds + \int_{CD}\boldsymbol{u}\cdot\boldsymbol{\tau}_{CD}ds + \int_{DA}\boldsymbol{u}\cdot\boldsymbol{\tau}_{DA}ds\right]\Big/(4l_1l_3\sin\alpha). \tag{2.24}$$

Using Lemma 2.6 in (2.24), we have

$$R(\nabla\times\boldsymbol{u}_I)(\boldsymbol{x}_e) = \partial_x u_2(\boldsymbol{x}_e) - \partial_y u_1(\boldsymbol{x}_e) + O(h^4)/4l_1l_3\sin\alpha = \nabla\times\boldsymbol{u}(\boldsymbol{x}_e) + O(h^2),$$

which concludes the proof. □

Using the same technique as above, we have proved the following pointwise superconvergence result between one function and its Nédélec interpolation in our early work [18].

Lemma 2.8 [18, Theorem 3.4]. *Under the same assumption as Lemma 2.6, for any function* $\boldsymbol{u} = (u_1, u_2)^T \in (W^{2,\infty}(\Omega))^2$ *and any parallelogram center* $\boldsymbol{x}_e$*, we have*

$$|\boldsymbol{u}(\boldsymbol{x}_e) - R(\boldsymbol{u}_I(\boldsymbol{x}_e))| \leqslant Ch^2.$$

With the above preparations, we can obtain the following superconvergence result between the analytic solution $\boldsymbol{E}$ of (2.6) and the postprocessed solution $\boldsymbol{E}_h$ of (2.9).

Theorem 2.2. *Assume that the domain* Ω *is covered by a triangular mesh formed by parallelograms, and* $\boldsymbol{E}$ *and* $\boldsymbol{E}_h$ *satisfy (2.6) and (2.9). If* $\boldsymbol{E} \in (W^{3,\infty}(\Omega))^2$ *and* h *is sufficiently small, then we have*

$$||\boldsymbol{E} - R(\boldsymbol{E}_h)||_{l_2,\Omega} + ||\nabla\times\boldsymbol{E} - R(\nabla\times\boldsymbol{E}_h)||_{l_2,\Omega} \leqslant Ch^2. \tag{2.25}$$

Proof. Using the triangle inequality, Lemmas 2.5, 2.8 and 2.7, we easily have

$$||\boldsymbol{E} - R(\boldsymbol{E}_h)||_{l_2,\Omega} + ||\nabla\times\boldsymbol{E} - R(\nabla\times\boldsymbol{E}_h)||_{l_2,\Omega} \leqslant \left(h^2||\boldsymbol{E}||_{(H^3(\Omega))^2} + h^{\delta+1/2}||e_h||_{H(curl;\Omega)}\right).$$

Letting $\delta = 1/2$ for a smooth solution and using Theorem 2.1, we complete the proof. □

3. Application to adaptive FE method for cloaking simulation

In the section, we will use the superconvergence results obtained above to an adaptive finite element method for cloaking simulation.

3.1. Model equations of electromagnetic cloaking

A very important property for Maxwell's equations is that Maxwell's equations are form invariant under coordinate transformations [31]. More specifically, under a coordinate transformation $\boldsymbol{x}' = \boldsymbol{x}'(\boldsymbol{x})$, the modeling Eqs. (2.1) and (2.2) keep the same form in the transformed space:

$$\nabla' \times \boldsymbol{E}' + i\omega\mu'\boldsymbol{H}' = \boldsymbol{0}, \tag{3.1}$$

$$\nabla' \times \boldsymbol{H}' - i\omega\varepsilon'\boldsymbol{E}' = \boldsymbol{0}, \tag{3.2}$$

where all new variables are given by

$$\boldsymbol{E}'(x') = A^{-T}\boldsymbol{E}(x), \quad \boldsymbol{H}'(x') = A^{-T}\boldsymbol{H}(x), \quad A = (A_{i,j}), \quad A_{i,j} = \frac{\partial x_i'}{\partial x_j} \tag{3.3}$$

and

$$\mu'(x') = A\mu A^T/det(A), \quad \varepsilon'(x') = A\varepsilon A^T/det(A). \tag{3.4}$$

Combining Eqs. (3.1) and (3.2) into an equation involving just one unknown $\boldsymbol{E}'$, we obtain:

$$\nabla' \times \left((\mu')^{-1}\nabla' \times \boldsymbol{E}'\right) - \omega^2\varepsilon'\boldsymbol{E}' = 0, \tag{3.5}$$

whose weak formulation is to find $\boldsymbol{E}' \in H_0(curl;\Omega')$ such that

$$b(\boldsymbol{E}', \boldsymbol{\phi}) \equiv ((\mu')^{-1}\nabla' \times \boldsymbol{E}', \nabla' \times \boldsymbol{\phi}) - \omega^2(\varepsilon'\boldsymbol{E}', \boldsymbol{\phi}) = 0 \quad \forall \boldsymbol{\phi} \in H_0(curl;\Omega). \tag{3.6}$$

3.2. The posterior error estimate

We use the recovery type a posterior error estimator

$$\eta = \left(\sum_{K\in T_h}\eta_K^2\right)^{1/2}, \tag{3.7}$$

where

$$\eta_K = \left(\frac{S_K}{3}\sum_{i=1}^{3}(\boldsymbol{E}_h(x_i) - R(E_h(x_i)))^2 + \frac{S_K}{3}\sum_{i=1}^{3}(\nabla \times \boldsymbol{E}_h(x_i) - R(\nabla \times \boldsymbol{E}_h(x_i)))^2\right)^{1/2}. \tag{3.8}$$

Here x_i $(i = 1, 2, 3)$ denote the midpoints of those three edges of element K.

For any function $\boldsymbol{u} \in H(curl;\Omega)$, denote

$$||\boldsymbol{u}||_{l_2,curl} = \left(\frac{S_K}{3}\sum_{i=1}^{3}|\boldsymbol{u}(\boldsymbol{x}_i)|^2 + \frac{S_K}{3}\sum_{i=1}^{3}|\nabla \times \boldsymbol{u}(\boldsymbol{x}_i)|^2\right)^{1/2}. \tag{3.9}$$

Theorem 3.1. *Under the same assumptions as Theorem 2.2, if there exists a constant $c(\boldsymbol{E}) > 0$ such that*

$$||\boldsymbol{E} - \boldsymbol{E}_h||_{l_2,curl} \geqslant c(\boldsymbol{E})h, \tag{3.10}$$

then there exists a constant $C > 0$ independent of h such that

$$\left|\frac{||R(\boldsymbol{E}_h) - \boldsymbol{E}_h||_{l_2,curl}}{||\boldsymbol{E} - \boldsymbol{E}_h||_{l_2,curl}} - 1\right| \leqslant Ch. \tag{3.11}$$

Proof. By Theorem 2.2, the definition (3.8), and the assumption (3.10), we have

$$\left|\frac{||R(\boldsymbol{E}_h) - \boldsymbol{E}_h||_{l_2,curl}}{||\boldsymbol{E} - \boldsymbol{E}_h||_{l_2,curl}} - 1\right| \leqslant \frac{||\boldsymbol{E} - R(\boldsymbol{E}_h)||_{l_2,curl}}{||\boldsymbol{E} - \boldsymbol{E}_h||_{l_2,curl}} \leqslant Ch, \tag{3.12}$$

which completes the proof. □

Theorem 3.1 shows that η is an asymptotically exact error estimator.

3.3. The adaptive finite element algorithm

The adaptive finite element algorithm for our cloaking simulation consists of the following steps:

Step 1. Solve (3.6) for the finite element solution $\boldsymbol{E}_h$ (for simplicity we drop the prime in the rest of the paper) on the mesh $\mathcal{T}_h$.

Step 2. For each edge mid-point x_e shared by two elements K_1 and K_2, calculate the postprocessed values $R(\boldsymbol{E}_h)(x_e) = \frac{1}{2}\left(\boldsymbol{E}_h(x_e)|_{K_1} + \boldsymbol{E}_h(x_e)|_{K_2}\right)$ and $R(\nabla \times \boldsymbol{E}_h(x_e)) = \frac{1}{2}\left(\nabla \times \boldsymbol{E}_h(x_e)|_{K_1} + \nabla \times \boldsymbol{E}_h(x_e)|_{K_2}\right)$.

Step 3. For each element, compute the recovery posterior error estimator η_K given by (3.8). Use it to direct how mesh gets refined and return to Step 1 until the error is within a given error tolerance.

There are many mesh adaptivity algorithms developed over the years, here we use a triangular mesh adaptivity algorithm that combines a posteriori error estimator with centroidal Voronoi–Delaunay tessellations (CVDT) of 2-D domains. In recent years CVDT has become a popular method to generate an adaptive mesh [13,14,22]. The CVDT method has two nice features: the solution errors are very well distributed over the triangles; the patch of each interior edge of the CVDT mesh forms nearly a parallelogram, which property leads to superconvergence [19,20]. Similar superconvergence estimates have been proved (e.g., [2]) for elliptic problems solved by piecewise linear finite elements on meshes where most pairs of triangles sharing a common edge form approximate parallelograms.

3.4. The PML equation

To restrict the wave propagation to a bounded domain, we adopt the perfectly matched layer (PML) concept originally introduced by Berenger [5] and further studied by many researchers (e.g., [3,6]).

The weak formulation of PML equation in the PML domain Ω_{pml} is given as [32]: Find $\boldsymbol{u} \in H_0(curl;\Omega_{pml})$ such that

$$a_{pml}(\boldsymbol{u},\boldsymbol{\psi}) \equiv \int_{\Omega_{pml}} \left[A\nabla \times \boldsymbol{u} \cdot \overline{\nabla \times \boldsymbol{\psi}} - B\boldsymbol{u} \cdot \boldsymbol{\psi}\right] d\boldsymbol{x} = 0 \quad \forall \boldsymbol{\psi} \in H_0(curl;\Omega_{pml}) \tag{3.13}$$

where $A = 1/(d(x)d(y))$, $B = \mathrm{diag}\left(\frac{d(y)}{d(x)}, \frac{d(x)}{d(y)}\right)$. Moreover, the stretching function $d(x) = 1 + i\sigma(x)$, and the absorption function $\sigma(x)$ is usually chosen as a polynomial function of the distance from the PML interface.

4. Numerical results

In this section, we present five numerical examples to justify our theoretical analysis and demonstrate the effectiveness of our adaptive edge element method used for cloaking simulations,

Example 1. This example is used to validate our theoretical analysis. For simplicity, we consider the domain $\Omega = [-1,1] \times [-1,1]$. To rigorously check the convergence rate, we construct the following analytical solution of (2.4) with $k = 1$:

$$\boldsymbol{E}(x,y) = (\cos(\pi x)\sin(\pi y), -\sin(\pi x)\cos(\pi y))^T,$$

which corresponds to a right hand source term

$$\boldsymbol{f}(x,y) = \left((2\pi^2 - 1)\cos(\pi x)\sin(\pi y), -(2\pi^2 - 1)\cos(\pi y)\sin(\pi x)\right)^T.$$

It is easy to see that the solution $\boldsymbol{E}$ satisfies the condition $\nabla \cdot \boldsymbol{E} = 0$ in Ω and the PEC boundary condition (2.5).

The obtained errors in the standard L_2 norm and the discrete l_2 norm are presented in Tables 4.1 and 4.2, respectively. Table 4.1 justifies the classical convergence result stated in Theorem 2.1. Results in Table 4.2 clearly show the superconvergence rates $O(h^2)$ for both $||\boldsymbol{E} - R(\boldsymbol{E}_h)||_{l_2}$ and $||\nabla \times \boldsymbol{E} - R(\nabla \times \boldsymbol{E}_h)||_{l_2}$, which are consistent with Theorem 2.2.

Example 2. This example is used to check the effectiveness of our a posterior error estimator (3.8) using an analytical solution. We consider the non-convex L-shaped domain $\Omega = [-1,1]^2 \setminus (0,1) \times (-1,0)$, and solve (2.4) with $k = 1$ and an exact solution given in polar coordinate system:

$$\boldsymbol{E}(r,\theta) = \nabla\left(r^{\beta} sin(\beta\theta)\right),$$

where $\beta = 2/3$. Note that the analytical solution $\boldsymbol{E}$ has a singularity at the re-entrant corner $(0,0)$ and only has regularity $(H^{\frac{2}{3}-\delta}(\Omega))^2$, where $\delta > 0$ is a very small number. Here we use the posterior error estimator η_K given by (3.8) to guide our adaptive finite element method. The obtained adaptive meshes and the convergences are illustrated in Fig. 4.1, where DoFs denote the total number of degrees of freedom (DoFs).

Example 3. This example is used to check the effectiveness of our a posterior error estimator (3.8) for an inhomogeneous medium problem. We choose domain $\Omega = [-1,1]^2$, $\omega = 1$, and the permittivity and permeability as follows:

Table 4.1
Example 1. The L_2 errors of $\boldsymbol{E}$ obtained on uniformly refined triangular meshes.

Meshes	$\|\|\boldsymbol{E}-\boldsymbol{E}_h\|\|_0$	Rate	$\|\|\nabla\times(\boldsymbol{E}-\boldsymbol{E}_h)\|\|_0$	Rate
$h = 1/4$	0.32298018117	–	1.61376416199	–
$h = 1/8$	0.16065007694	1.0075	0.81852582872	0.9793
$h = 1/16$	0.08020204442	1.0022	0.41073945140	0.9948
$h = 1/32$	0.04008505709	1.0005	0.20555495590	0.9986
$h = 1/64$	0.02004051420	1.0001	0.10280065248	0.9996

Table 4.2
Example 1. The discrete l_2 errors of $\boldsymbol{E}$ obtained on uniformly refined triangular meshes.

Meshes	$\|\|\boldsymbol{E}-R(\boldsymbol{E}_h)\|\|_{l_2}$	Rate	$\|\|\nabla\times\boldsymbol{E}-R(\nabla\times\boldsymbol{E}_h)\|\|_{l_2}$	Rate
$h = 1/4$	0.24025530848	–	1.61376416199	–
$h = 1/8$	0.06330436740	1.9241	0.81852582872	1.9085
$h = 1/16$	0.01609920045	1.9753	0.41073945140	1.9701
$h = 1/32$	0.00405015056	1.9909	0.20555495590	1.9890
$h = 1/64$	0.00101514630	1.9962	0.10280065248	1.9954

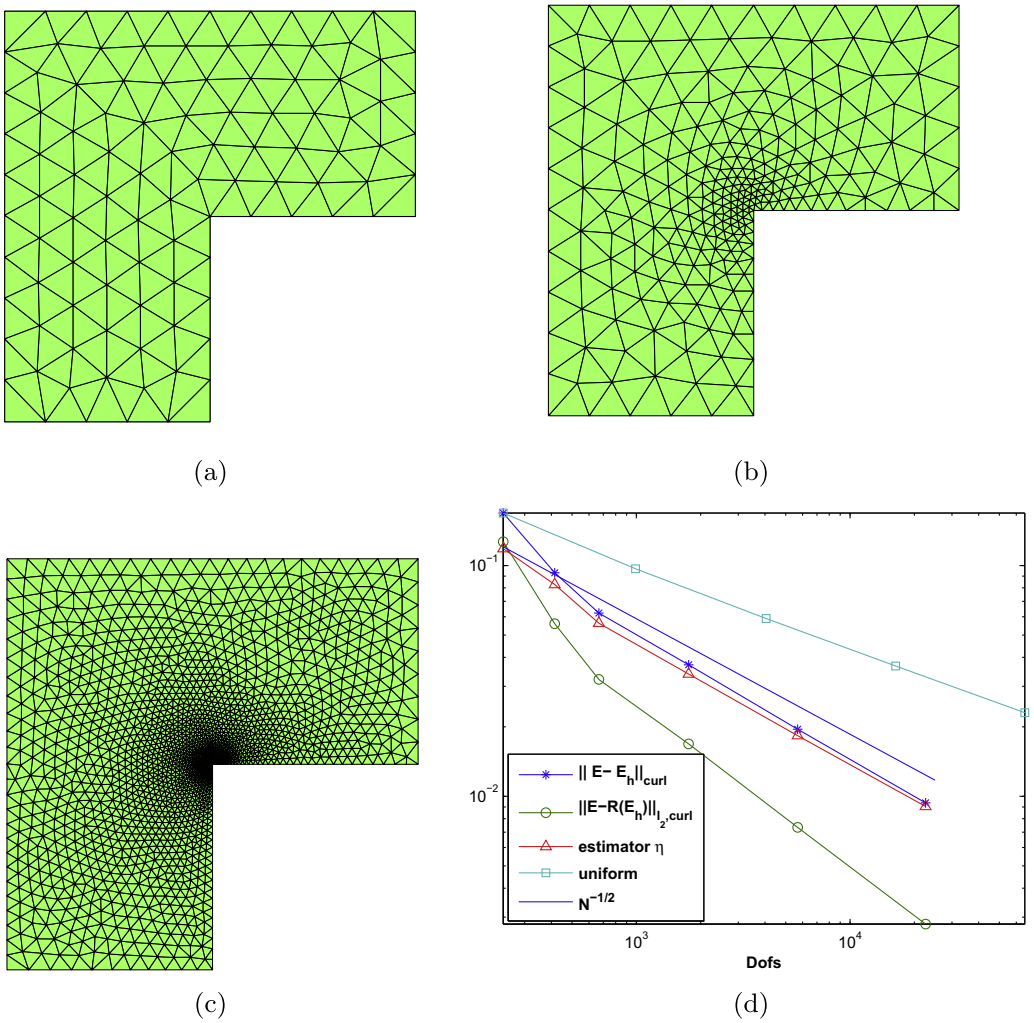

Fig. 4.1. Example 2. (a) The initial mesh; (b) the mesh after 2 adaptive refinements (668 DoFs); (c) the mesh after 4 adaptive refinements (5682 DoFs) and (d) comparison of errors on uniformly refined meshes and adaptive meshes.

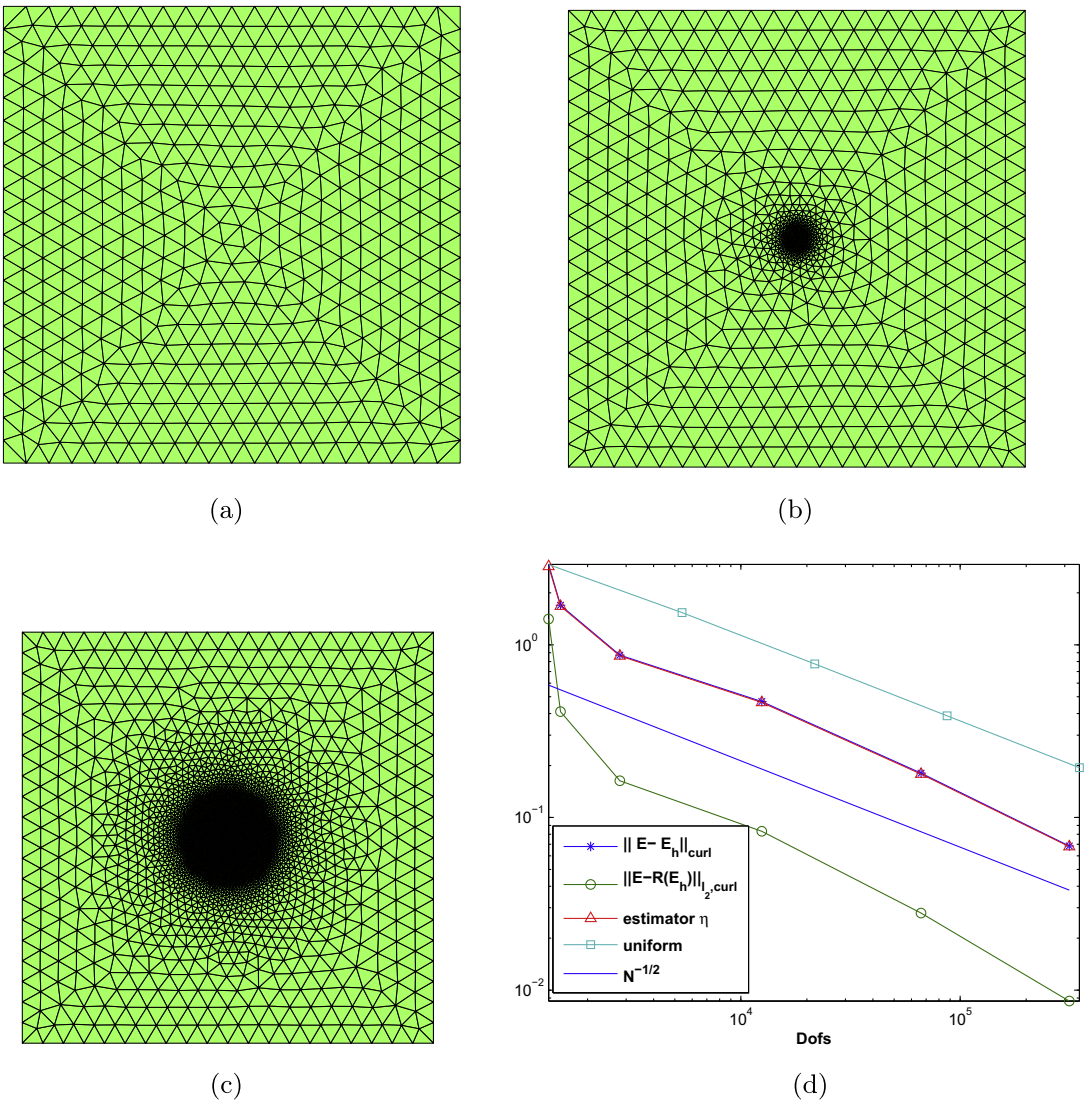

Fig. 4.2. Example 3. (a) The initial mesh (1328 DoFs); (b) the adaptive mesh after 2 refinements (2807 DoFs); (c) the adaptive mesh after 4 refinements (66,329 DoFs) and (d) the errors obtained on uniformly refined meshes and adaptive meshes.

$$\varepsilon = \begin{pmatrix} 1+x^2 & xy \\ xy & 1+y^2 \end{pmatrix}, \quad \mu = \frac{1}{1+x^2+y^2}$$

such that (2.3) has an exact solution

$$\boldsymbol{E} = \begin{pmatrix} \frac{y}{x^2+y^2+0.02} \\ \frac{-x}{x^2+y^2+0.02} \end{pmatrix}.$$

Note that the solution $\boldsymbol{E}$ satisfies the condition $\nabla \cdot \boldsymbol{E} = 0$ in Ω. The source term of (2.3) is obtained by this exact $\boldsymbol{E}$. Selected adaptive meshes and the errors are illustrated in Fig. 4.2. Note that the adaptive meshes match the behavior of the analytical solution $\boldsymbol{E}$, which is shown in Fig. 4.3.

Example 4. Here we solve a cylindrical cloaking problem designed by Pendry et al. [33]. We select the domain $\Omega = [-2,2] \times [-2,2]$, a cloaked object is put inside a perfectly conducting cylinder with radius $R_1 = 0.3$ m, then the cylinder is wrapped by a cylindrical cloak with thickness $R_2 - R_1$, where $R_2 = 0.6$ m. The cloak is made with a metamaterial, whose permeability and permittivity are given by Li and Huang [26]: For any $R_1 < r \leqslant R_2,\ 0 \leqslant \theta \leqslant 2\pi$,

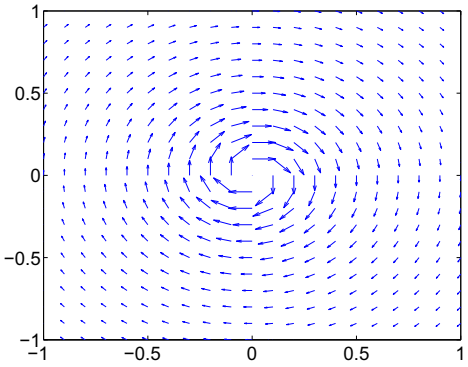

Fig. 4.3. Example 3. The exact solution $\boldsymbol{E}$.

$$
\begin{aligned}
\mu &= 1/\det(A),\\
\epsilon_{xx} &= \left[\left(\frac{R_2-R_1}{R_2}\right)^2 + \left(1+2\left(\frac{R_2-R_1}{R_2}\right)^2\frac{R_1}{r-R_1}\right)\sin^2\theta\right]\mu,\\
\epsilon_{xy} &= \epsilon_{yx} = -\left[\left(1+2\left(\frac{R_2-R_1}{R_2}\right)^2\frac{R_1}{r-R_1}\right)\sin\theta\cos\theta\right]\mu,\\
\epsilon_{yy} &= \left[\left(\frac{R_2-R_1}{R_2}\right)^2 + \left(1+2\left(\frac{R_2-R_1}{R_2}\right)^2\frac{R_1}{r-R_1}\right)\cos^2\theta\right]\mu,
\end{aligned}
$$

where

$$\det(A) = \left(\frac{R_2-R_1}{R_2}\right)^2\cdot\frac{r}{r-R_1}.$$

To model the cloaking phenomenon, we use a PML around the outside of the physical domain. More specifically, here our PML domain is chosen to be $\Omega\setminus[-1.5,1.5]\times[-1.5,1.5]$. The absorption function $\sigma(x)$ is chosen as a linear function, i.e.,

$$\sigma(x) = \begin{cases} 1, & \text{if } |x|>1.75,\\ 4(|x|-1.5), & \text{if } 1.5\leqslant|x|\leqslant 1.75,\\ 0, & \text{if } |x|<1.5. \end{cases} \tag{4.1}$$

The cloaking simulation obtained using our adaptive method is illustrated in Fig. 4.4, which shows clearly that our adaptive algorithm works effectively.

Example 5. Encouraged by our adaptive results obtained for the cylindrical cloak. We further apply the adaptive algorithm to a triangle cloak, which is more challenging, since we have sharp corners in this case.

For this example, we choose the domain $\Omega=[-2,2]\times[-2,2]$, the cloaked object is put inside a PEC triangle, whose vertices are $a\left(\sin\frac{2(i-1)\pi}{3},\cos\frac{2(i-1)\pi}{3}\right)$, $i=1,2,3$. Then this triangle is wrapped by a triangular cloak, whose vertices are given by points $b\left(\sin\frac{2(i-1)\pi}{3},\cos\frac{2(i-1)\pi}{3}\right)$, $i=1,2,3$, where $a=0.2$ and $b=0.6$ are the radii of the circumcircles of the inner and outer triangles, respectively. The permeability and permittivity of the cloak are given by Wu et al. [37]:

$$
\begin{aligned}
\mu &= \left(m_1^2+\frac{am_1}{2|r_1|}\right)^{-1},\\
\varepsilon_{xx} &= \left[m_1^2 + am_1\frac{\cos\frac{(2i-1)\pi}{3}}{r_1|r_1|}y + \left(\frac{a}{2}\cos\left(\frac{(2i-1)\pi}{3}\right)\right)^2\frac{x^2+y^2}{r_1^4}\right]\mu,\\
\varepsilon_{xy} &= \varepsilon_{yx} = \left[-\frac{am_1\left(y\sin\left(\frac{(2i-1)\pi}{3}\right)+x\cos\left(\frac{(2i-1)\pi}{3}\right)\right)}{2r_1|r_1|} - \frac{a^2\sin\left(\frac{(2i-1)\pi}{3}\right)\cos\left(\frac{(2i-1)\pi}{3}\right)(x^2+y^2)}{4r_1^4}\right]\mu,\\
\varepsilon_{yy} &= \left[m_1^2 + 2am_1m_2\frac{\sin\frac{(2i-1)\pi}{3}}{r_1|r_1|}x + \left(am_2\sin(\frac{(2i-1)\pi}{3})\right)^2\frac{x^2+y^2}{r_1^4}\right]\mu,
\end{aligned}
$$

where $m_1=\frac{b-a}{a}$, $m_2=\cos\frac{\pi}{3}$, and $r_1=y\cos\left(\frac{(2i-1)\pi}{3}\right)+x\sin(\frac{(2i-1)\pi}{3})$, $i=1,2,3$.

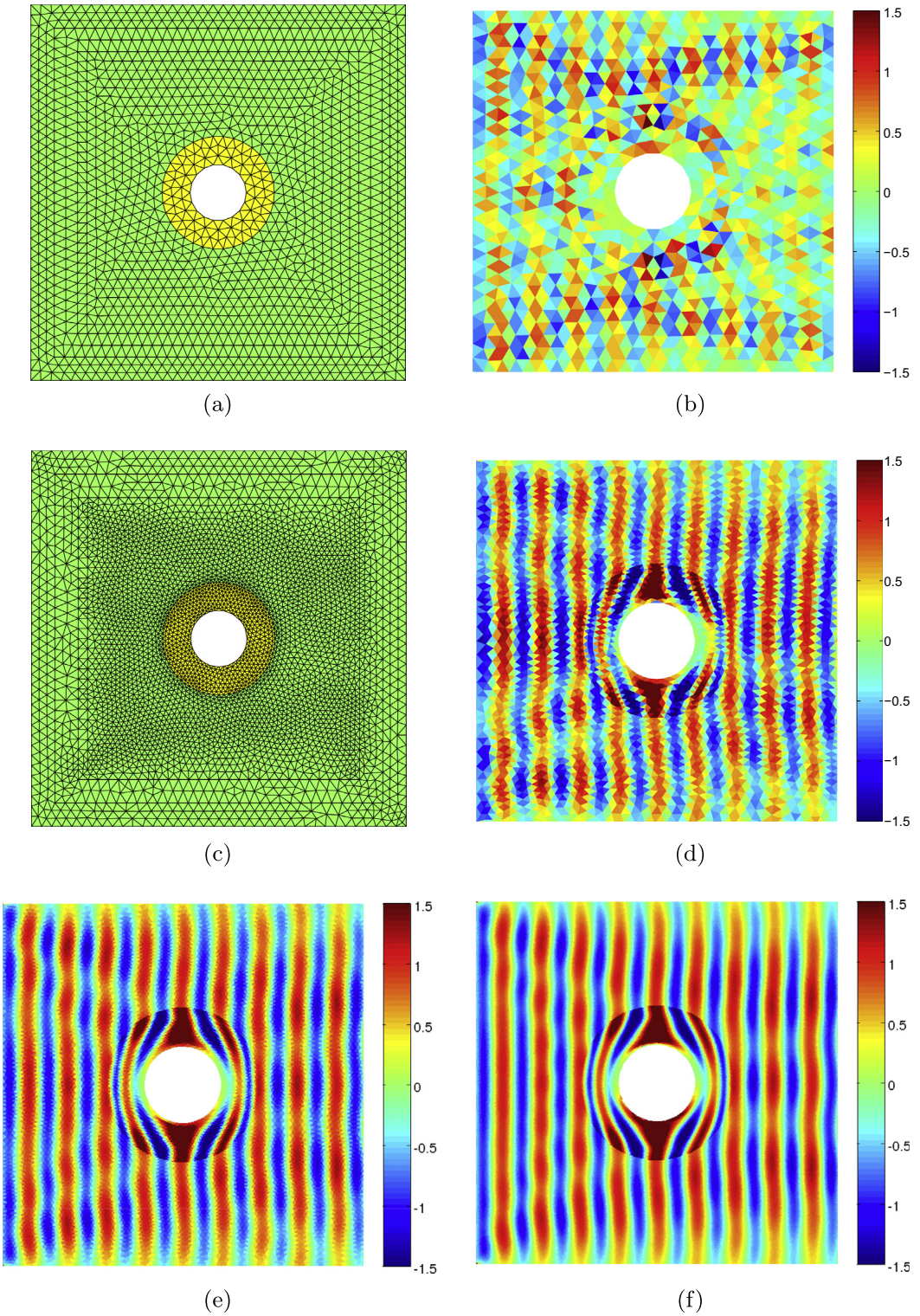

Fig. 4.4. Example 4. (a) The initial mesh (2956 elements, 4351 DoFs); (b) the real part of $\boldsymbol{E}$ obtained on (a); (c) the mesh after 4 refinements (6390 elements, 9498 DoFs); (d) the real part of $\boldsymbol{E}$ obtained on (c); (e) The real part of $\boldsymbol{E}$ after 10 refinements (29,110 elements, 43,551 DoF) and (f) the real part of $\boldsymbol{E}$ after 16 refinements (156,443 elements, 234,504 DoFs).

The obtained cloaking simulation is illustrated in Fig. 4.5, which demonstrates that our adaptive algorithm works effectively even when the cloak has sharp corners.

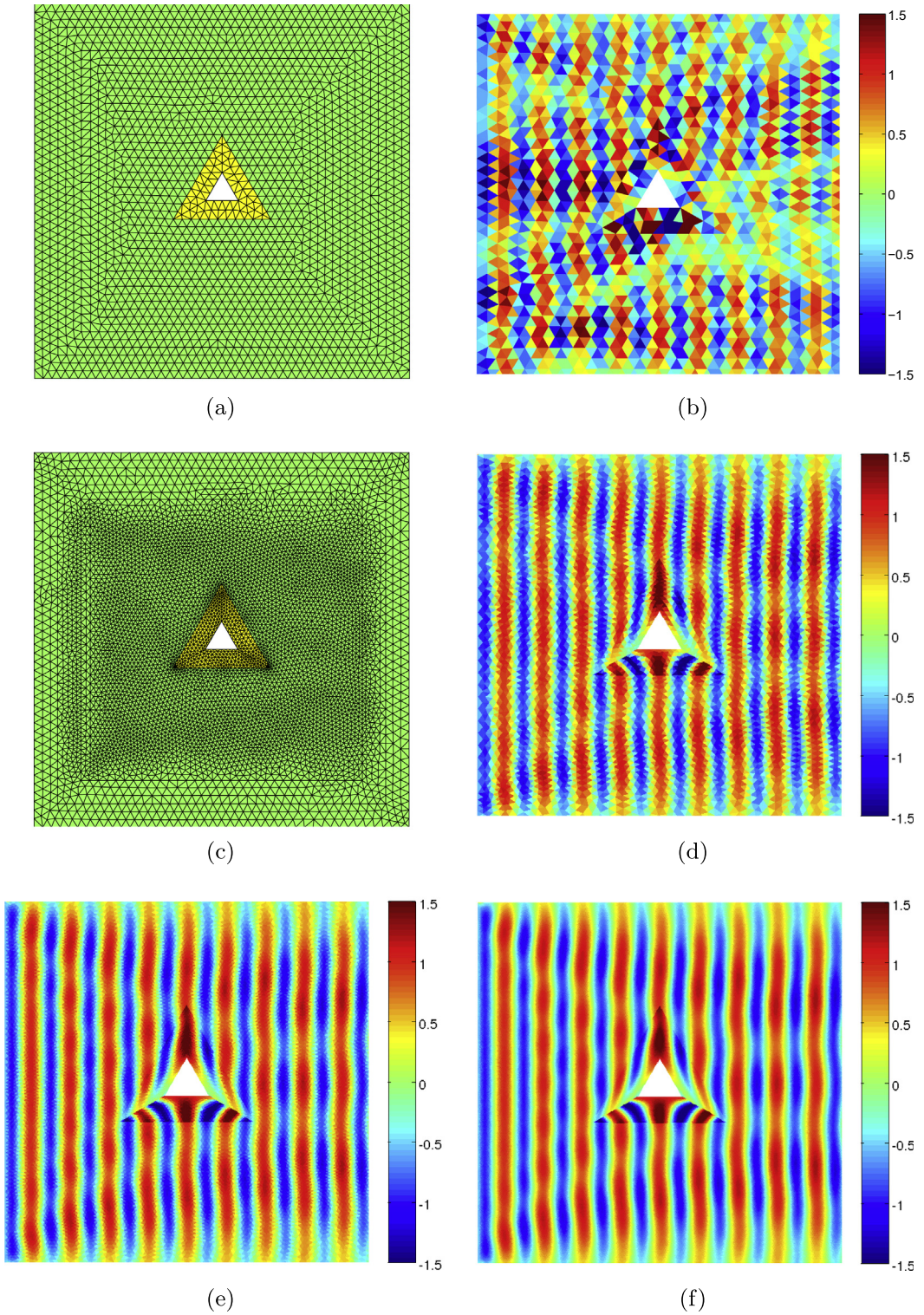

Fig. 4.5. Example 5. (a) The initial mesh (4126 elements, 6097 DoFs); (b) the real part of $\boldsymbol{E}$ obtained on (a); (c) the mesh after 5 refinements (12,343 elements, 18,417 DoFs); (d) the real part of $\boldsymbol{E}$ obtained on (c); (e) The real part of $\boldsymbol{E}$ after 9 refinements (35,624 elements, 53,328 DoFs) and (f) the real part of $\boldsymbol{E}$ after 14 refinements (145,806 elements, 218,582 DoFs).

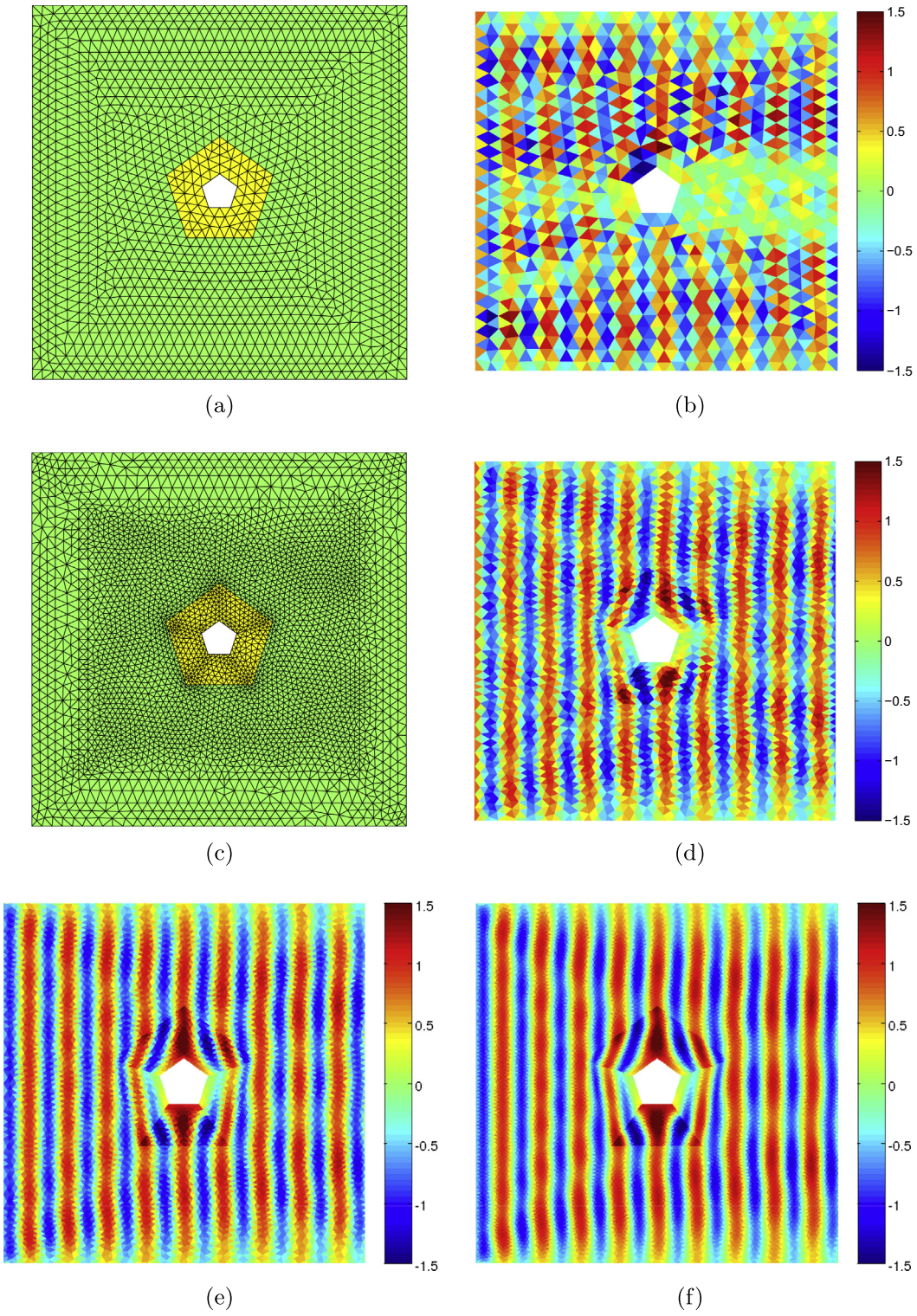

Fig. 4.6. Example 6. (a) The initial mesh (3026 elements, 4460 DoFs); (b) the real part of $\boldsymbol{E}$ obtained on (a); (c) the mesh after 4 refinements (6972 elements, 10,374 DoFs); (d) the real part of $\boldsymbol{E}$ obtained on (c); (e) the real part of $\boldsymbol{E}$ after 7 refinements (14,966 elements, 22,355 DoFs) and (f) the real part of $\boldsymbol{E}$ after 10 refinements (33,860 elements, 50,688 DoFs).

Example 6. Our last example is to apply the adaptive algorithm to a pentagonal cloak. For this example, we choose the domain $\Omega = [-2,2]\times[-2,2]$, and the cloaked object is put inside a PEC pentagon, which has vertices $a\left(\sin\frac{2(i-1)\pi}{5}, \cos\frac{2(i-1)\pi}{5}\right)$, $i = 1,2,3,4,5$. This pentagon is then wrapped by another pentagon cloak, whose vertices are $b\left(\sin\frac{2(i-1)\pi}{5}, \cos\frac{2(i-1)\pi}{5}\right)$, $i = 1,2,3,4,5$, where $a = 0.2$ and $b = 0.6$ are the radii of the circumcircles of the inner and outer pentagons. The cloak's permeability and permittivity are given by Wu et al. [37]:

$$\mu = \left(m_1^2 + \frac{am_1m_2)}{|r_1|}\right)^{-1},$$

$$\varepsilon_{xx} = \left[m_1^2 + 2am_1m_2\frac{\cos\frac{(2i-1)\pi}{5}}{r_1|r_1|}y + \left(am_2\cos\left(\frac{(2i-1)\pi}{5}\right)\right)^2\frac{x^2+y^2}{r_1^4}\right]\mu,$$

$$\varepsilon_{xy} = \varepsilon_{yx} = -\left[\frac{am_1m_2\left(y\sin\left(\frac{(2i-1)\pi}{5}\right) + x\cos\left(\frac{(2i-1)\pi}{5}\right)\right)}{r_1|r_1|} + \frac{(am_2)^2\sin\left(\frac{(2i-1)\pi}{5}\right)\cos\left(\frac{(2i-1)\pi}{5}\right)(x^2+y^2)}{r_1^4}\right]\mu,$$

$$\varepsilon_{yy} = \left[m_1^2 + 2am_1m_2\frac{\sin\frac{(2i-1)\pi}{5}}{r_1|r_1|}x + \left(am_2\sin\left(\frac{(2i-1)\pi}{5}\right)\right)^2\frac{x^2+y^2}{r_1^4}\right]\mu,$$

where $m_1 = \frac{b-a}{a}$, $m_2 = cos(\frac{\pi}{5})$, and $r_1 = y\cos\left(\frac{(2i-1)\pi}{5}\right) + x\sin\left(\frac{(2i-1)\pi}{5}\right)$, $i = 1,2,3,4,5$.

For this example, we also obtained excellent cloaking phenomenon illustrated in Fig. 4.6, which further demonstrates that our adaptive algorithm works effectively for this pentagonal cloak.

5. Conclusions

In this paper, we present an efficient adaptive finite element method for the time-harmonic Maxwell's equations. The mesh adaptivity is guided by the recovery type a posteriori error estimator based on the superconvergence result proved for the lowest triangular edge element. Various numerical experiments are carried out and demonstrate that our method works effectively even for cloaking simulations where the permittivity and permeability are highly anisotropic coefficients. Rigorous proof of superconvergence in this case is very technical compared to the constant coefficient case, detailed proof will be given in a separate theoretical paper.

Acknowledgments

The authors are very grateful to two referees for their insightful comments which improve the paper.

References

[1] M. Ainsworth, J. Coyle, Hierarchic *hp*-edge element families for Maxwell's equations on hybrid quadrilateral/triangular meshes, Comput. Methods Appl. Mech. Eng. 190 (2001) 6709–6733.
[2] R.E. Bank, J. Xu, Asymptotically exact a posterior error estimates. Part I: Grids with superconvergence, SIAM J. Numer. Anal. 41 (2003) 2294–2312.
[3] G. Bao, P. Li, H. Wu, An adaptive edge element with perfectly matched absorbing layers for wave scattering by biperiodic structures, Math. Comput. 79 (2010) 1–34.
[4] R. Beck, P. Deuflhard, R. Hiptmair, R.H.W. Hoppe, B. Wohlmuth, Adaptive multilevel methods for edge element discretizations of Maxwells equations, Surv. Math. Ind. 8 (1999) 271–312.
[5] J.P. Berenger, A perfectly matched layer for the absorption of electromagnetic waves, J. Comput. Phys. 114 (1994) 185–200.
[6] J. Bramble, J. Pasciak, Analysis of a cartesian PML approximation to the three dimensional electromagnetic wave scattering problem, Int. J. Numer. Anal. Model. 9 (3) (2012) 543–561.
[7] C. Carstensen, M. Eigel, R.H.W. Hoppe, C. Löbhard, A review of unified a posteriori finite element error control, Numer. Math. Theor. Methods Appl. 5 (2012) 509–558.
[8] H. Chen, C.T. Chan, P. Sheng, Transformation optics and metamaterials, Nat. Mater. 9 (2010) 387–396.
[9] J. Chen, Y. Xu, J. Zou, Convergence analysis of an adaptive edge element method for Maxwell's equations, Appl. Numer. Math. 59 (2009) 2950–2969.
[10] Z. Chen, L. Wang, W. Zheng, An adaptive multilevel method for time-harmonic Maxwell equations with singularities, SIAM J. Sci. Comput. 29 (2007) 118–138.
[11] L. Demkowicz, J. Kurtz, D. Pardo, M. Paszynski, W. Rachowicz, A. Zdunek, Computing with Hp-Adaptive Finite Elements, Frontiers: Three Dimensional Elliptic and Maxwell Problems with Applications, vol. 2, CRC Press, Boca Raton, 2007.
[12] L. Demkowicz, J. Li, Numerical simulations of cloaking problems using a DPG method, Comput. Mech. 51 (2013) 661–672, doi: 10.1007/s00466-012-0744-4.
[13] Q. Du, V. Faber, M. Gunzburger, Centroidal Voronoi tessellations: applications and algorithms, SIAM Rev. 41 (1999) 637–676.
[14] Q. Du, M. Gunzburger, L. Ju, Adances in studies and applications of Centroidal Voronoi tessellations, Numer. Math. Theor. Methods 3 (2010) 119–142.
[15] A. Greenleaf, Y. Kurylev, M. Lassas, G. Uhlmann, Cloaking devices, electromagnetics wormholes and transformation optics, SIAM Rev. 51 (2009) 3–33.
[16] S. Guenneau, R.C. McPhedran, S. Enoch, A.B. Movchan, M. Farhat, N.-A.P. Nicorovici, The colours of cloaks, J. Opt. 13 (2011) 024014.
[17] Y. Huang, J. Li, Q. Lin, Superconvergence analysis for time-dependent Maxwell's equations in metamaterials, Numer. Methods Part. Differ. Equ. 28 (2012) 1794–1816.
[18] Y. Huang, J. Li, C. Wu, The averaging technique for superconvergence: verification and application of 2D edge elements to Maxwell's equations in metamaterials, Comput. Methods Appl. Mech. Eng. 255 (2013) 121–132.
[19] Y. Huang, H. Qin, D. Wang, Centroidal Voronoi tessellation-based finite element superconvergence, Internat. J. Numer. Methods Eng. 76 (2008) 1819–1839.
[20] Y. Huang, H. Qin, D. Wang, Q. Du, Convergent adaptive finite element method based on centroidal Voronoi tessellations and superconvergence, Commun. Comput. Phys. 10 (2011) 339–370.

[21] X. Jiang, P. Li, W. Zheng, Numerical solution of acoustic scattering by an adaptive DtN finite element method, Commun. Comput. Phys. 13 (2013) 1227–1244.
[22] L. Ju, M. Gunzburger, W. Zhao, Adaptive finite element methods for elliptic PDEs based on conforming centroidal Voronoi–Delaunay triangulations, SIAM. J. Sci. Comput. 28 (2006) 2023–2053.
[23] R.V. Kohn, D. Onofrei, M.S. Vogelius, M.I. Weinstein, Cloaking via change of variables for the Helmholtz equation, Comm. Pure Appl. Math. 63 (2010) 0973–1016.
[24] U. Leonhardt, Optical conformal mapping, Science 312 (2006) 1777–1780.
[25] J. Li, Y. Chen, Computational Partial Differential Equations Using MATLAB, CRC Press, Boca Raton, 2008.
[26] J. Li, Y. Huang, Mathematical simulation of cloaking metamaterial structures, Adv. Appl. Math. Mech. 4 (2012) 93–101.
[27] J. Li, Y. Huang, Time-Domain Finite Element Methods for Maxwell's Equations in Metamaterials, Springer Series in Computational Mathematics, vol. 43, Springer, 2013.
[28] J. Li, Y. Huang, W. Yang, Developing a time-domain finite-element method for modeling of electromagnetic cylindrical cloaks, J. Comput. Phys. 231 (2012) 2880–2891.
[29] H. Liu, T. Zhou, On approximate electromagnetic cloaking by transformation media, SIAM J. Appl. Math. 71 (2011) 218–241.
[30] J. McGuirk, P. Collins, M. Havrilla, A. Wood, A Green's function approach to calculate scattering width for cylindrical cloaks, Appl. Comput. Electromagnet. Soc. J. 25 (2010) 108–116.
[31] G.W. Milton, M. Briane, J.R. Willis, On cloaking for elasticity and physical equations with a transformation invariant form, New J. Phys. 8 (2006) 248.
[32] P. Monk, Finite Element Methods for Maxwell's Equations, Oxford University Press, 2003.
[33] J.B. Pendry, D. Schurig, D.R. Smith, Controlling electromagnetic fields, Science 312 (2006) 1780–1782.
[34] Z. Qiao, C. Yao, S. Jia, Superconvergence and extrapolation analysis of a nonconforming mixed finite element approximation for time-harmonic Maxwell's equations, J. Sci. Comput. 46 (2011) 1–19.
[35] D. Schurig, J.J. Mock, B.J. Justice, S.A. Cummer, J.B. Pendry, A.F. Starr, D.R. Smith, Metamaterial electromagnetic cloak at microwave frequencies, Science 314 (2006) 977–980.
[36] P. Solin, L. Dubcova, J. Cerveny, I. Dolezel, Adaptive hp-FEM with arbitrary-level hanging nodes for Maxwell's equations, Adv. Appl. Math. Mech. 2 (2010) 518–532.
[37] Q. Wu, K. Zhang, F. Meng, L. Li, Material parameters characterization for arbitrary N-side regular polygonal invisible cloak, J. Phys. D: Appl. Phys. 42 (2009).
[38] J. Xu, Z.M. Zhang, Analysis of recovery type a posteriori error estimators for mildly structured grids, Math. Comput. 73 (2003) 781–801.
[39] N. Yan, A. Zhou, Gradient recovery type a posteriori error estimates for finite element approximations on irregular meshes, Comput. Methods Appl. Mech. Eng. 190 (2001) 4289–4299.
[40] Y.B. Zhai, X.W. Ping, W.X. Jiang, T.J. Cui, Finite-element analysis of three-dimensional axisymmetrical invisibility cloaks and other metamaterial devices, Commun. Comput. Phys. 4 (2010) 823–834.
[41] L. Zhong, L. Chen, S. Shu, G. Wittum, J. Xu, Convergence and optimality of adaptive edge finite element methods for time-harmonic Maxwell equations, Math. Comput. 81 (2012) 623–642.
[42] O.C. Zienkiewicz, J.Z. Zhu, A simple error estimator and adaptive procedure for practical engineering analysis, Int. J. Numer. Methods Eng. 24 (1987) 337–357.